Original Study **Open Access**

Armand Augustin Fondjo*, Sai K. Vanapalli, Richard P. Ray, Elizabeth Theron

Relationships between Shear Strength Parameters with Mineralogy and Index Properties of Compacted, Unsaturated Soils

https://doi.org/10.2478/sgem-2025-0006
received June 19, 2024; accepted November 23, 2024.

Abstract: The objective of this study is to assess the influences of soil index properties, swelling parameters, and soil mineralogy on unsaturated shear strength parameters (ϕ‘, ϕ^b, c‘) of compacted expansive soils. The laboratory tests include the grain size distribution, specific gravity (Gs), Atterberg limits, swelling potential, X-ray diffraction, modified Proctor compaction, soil suction, and triaxial testing. MINITAB 19 statistical analysis software generates the tri-dimensional surface graphs. The values ϕ‘, ϕ^b, and c‘ are majorly influenced by water (%), Gs, and clay (%). ϕ‘ shows a strong correlation with free swell ratio (FSR), free swell index (FSI), and void ratio. ϕ^b demonstrates a strong relationship with liquid limit, plasticity index, and γ_d (dry unit weight). ϕ‘ and c‘ portray a moderate relationship with liquid limit, plasticity limit, and γ_d. ϕ‘ exhibits a moderate correlation with smectite (%) and plagioclase (%). ϕ^b describes a strong relationship with smectite (%) and a moderate correlation with plagioclase and K-feldspar (%). c‘ depicts a moderate correlation with smectite (%), K-feldspar (%), and plagioclase (%). The matric suction controls the behaviour of unsaturated soils. Nonetheless, the influences of soil index properties, swelling potential, and mineralogy on shear strength are not marginal. These findings provide a good insight into the behaviour of unsaturated expansive soils and contribute to enhancing geotechnical modelling.

***Corresponding author: Armand Augustin Fondjo,** Department of Civil Engineering. Faculty of Engineering, Built Environment & Information Technology. Central University of Technology, Free State, South Africa, E-mail: fondjoarmand1976@gmail.com
Sai K. Vanapalli, Department of Civil Engineering, University of Ottawa, Canada
Richard P. Ray, Structural and Geotechnical Engineering Department, Széchenyi István Egyetem University, 9026 Gyor, Egyetem tér 1, Hungary
Elizabeth Theron, Department of Civil Engineering. Faculty of Engineering, Built Environment & Information Technology. Central University of Technology, Free State, South Africa

Keywords: Expansive soils; shear strength; matric suction; soil index properties; swelling potential; soil mineralogy.

1 Introduction

Expansive soils are highly plastic materials containing a relevant fraction of clay silt and are very sensitive to water variation [1, 2, 3, 4, 5, 78]. The problems related to expansive soils can be evaluated through the concept of unsaturated soil mechanics because the hydro-mechanical behaviour of expansive soils is governed essentially by the principle of soil suction to a large extent [6, 7]. The shear strength is a significant parameter of soil material, and the design of engineered structures relies on the shear strength and stiffness of the soil support [8, 4, 9, 79]. Terzaghi [80] used the effective stress variable and the Mohr–Coulomb failure criterion [81] to formulate a mathematical equation to predict the shear strength of saturated soils given by Equation 1 in Appendix 6. The shear strength for unsaturated soils was developed as an extension of the saturated condition. The contribution of the matric suction is commonly added to the shear strength equation of saturated soil material to describe the shear strength of unsaturated soils. Equation 2 in Appendix 6 used in this study describes the shear strength of unsaturated soils as proposed by Fredlund and Rahardjo [60]. Other researchers such as Vanapalli *et al.* [27], Khalili and Khabbaz [25], Vanapalli and Fredlund [18], Tekinsoy *et al.* [28], Garven and Vanapalli [19], and Guan *et al.* [29] developed Equations 3 through 8, respectively, in Appendix 6 to predict the unsaturated shear strength. Researchers reported the influences of soil index properties and mineralogy on the shear strength of expansive soils. Sailie and Bucher [10], Calabresi and Scarpelli [11], Toll [12], Stark and Duncan [13], Chen et *al.* [14], Chowdhury [15], Domitrović and Zelić [16] stated that water content portrays a significant influence on

shear strength, and the shear strength reduces when water content increases in expansive soils. In a similar study, Wang et *al*. [17] mentioned that the cohesion and friction angle reduces when the water content increases and exhibits a higher strength logarithmic correlation with a determination coefficient of $R^2 > 0.9$. Vanapalli and Fredlund [18], Garven and Vanapalli [19], and Chowdhury [15] investigated the influence of the plasticity index on shear strength of unsaturated soils. The results show that the plasticity index of soil mass exhibits an influence on the shear strength of unsaturated soils. Escario [20], Escario et *al*. [21], Chen et *al*. [14], and Chowdhury [15] reported that the dry unit weight of soil influences the shear strength of expansive unsaturated soils, and the shear strength increases when the dry unit weight increases. Another research work conducted by [22, 23] revealed that the shear strength of unsaturated soil reduces when the degree of saturation increases and the degree of saturation significantly influences the shear strength of expansive soils. Warkentin and Yong [24], and Wang et *al*. [17] pointed out that the shear strength of expansive soils reduces when the void ratio increases and the void ratio portrays an important influence on the shear strength of the soil material. Khalili and Khabbaz [25], Escario et *al*. [21], Gan et *al*. [26], Vanapalli et *al*. [27], Tekinsoy et *al*. [28], and Guan et *al*. [29] studied the effect of the air entry value (AEV) on shear strength. The findings indicated that the AEV influences the relationship between the shear strength and the matric suction and portrays a linear relationship when $u_a - u_w < AEV$ and a non-linear when $u_a - u_w > AEV$. Another research work conducted by [24, 20, 30, 31] revealed that the fraction and type of clay mineral significantly influence the shear strength of expansive soils, and the shear strength reduces when the quantity of clay mineral increases. The calcium montmorillonite shear strength is smaller than the sodium montmorillonite shear strength of an identical volume ratio. It appeared that few studies were reported on the influence of soil index properties and soil mineralogy on unsaturated shear strength parameters of expansive soils. The investigation of the influences of soil index properties and mineralogy on shear strength parameters (ϕ', ϕ^b, c') of compacted, unsaturated expansive soils contributes to a good insight into the behaviour of expansive soils.

2 Methods

2.1 Sampling locations

Four different soil samples were collected across Free State Province, South Africa. Workers excavated the pits manually using shovels and pickaxes and retrieved samples within the active zone depth. Samples were labelled as Bloemfontein (BFS), Welkom (WES), Winburg (WIS) and Bethlehem (BES) soils. Field crews adhered to standard sampling practices to preserve and transport soil samples. Table 1 in Appendix 1 shows the global positioning system (GPS) coordinates of sampling locations, and Figure 1 shows the map of the country/region where the soil samples were collected.

2.2 Laboratory testing

The testing program was designed to determine the physical and hydro-mechanical characteristics of the soil samples. The tests included gathering samples and field water content, following the standard practice for preserving and transporting samples [32]. Water content determination was performed [33], along with particle size analysis using a sieve [34] and sedimentation method [35]. Index and plasticity tests included the specific gravity [36] and consistency limits tests [37]. In addition, the free swell index test [38] and the free swell ratio test [39] were conducted. The water-density relationship was evaluated through the Modified Proctor compaction test [40], while mineralogy was analyzed through X-ray diffraction testing [41]. Unsaturated pore pressures were measured using the filter paper technique [42], and soil-water characteristic curve modeling was performed [43, 44, 45, 77, 46]. Finally, the triaxial Consolidated-Undrained tests help to measure the soil shear strength [47].

2.2.1 Sample preparation

Each sample (BFS, WES, WIS, BES) yielded five compacted specimens with different water content and dry unit weights, ranging from the dry side, optimum water content, and wet side of compacting curves. Dividing the four soil samples into twenty compacted specimens supplied the soil suction test and consolidated undrained test. The laboratory estimated the consistent results by averaging two for each tested specimen.

Figure 1: Sampling location map (https://www.exploresouthafrica.net/map/).

2.2.2 Free swell ratio

The free swell ratio (FSR) is the ratio of the equilibrium sediment volume of 10 g oven-dried soil passing through a 425-µm sieve in distilled water versus kerosene, as described in Equation 9. V_d is the volume (ml) of soil specimen in water, and V_k (ml) is the volume (ml) of soil specimen in kerosene. Sridharan and Prakash [39] proposed the method for the free swell ratio test. Table 2 in Appendix 1 provides information on the swelling potential and soil mineralogy.

$$FSR = \frac{V_d}{V_K} \tag{9}$$

2.2.3 Soil suction measurement

The soil suction measurement using a filter paper was conducted according to the standard [42]. A sharpened drive cylinder pushed into the compacted soil specimen, producing a cylindrical sub-specimen, 75 mm in diameter and 70 mm long for the soil suction test. Cutting the soil specimen in half allowed the best contact with the filter paper for matric suction measurement, with the top half in place, an electrical tape provided an outer seal around the filter paper–specimen interface, and the specimen was placed in a glass jar. A clean PVC O-ring with a sharp edge was inserted, facing up, on top of the soil specimen. The non-contact filter paper was placed over the PVC O-ring for total suction measurement. The glass jars were sealed using an airtight lid to prevent moisture exchange. The glass jars were labelled and placed in a temperature-controlled ice chest for an equilibrium time of 3 weeks. After the equilibrium time was completed, the filter papers were retrieved and weighed. The water contents W_f in non-contact and contact filter paper were calculated using Equation 10 for total and matric suction measurements, respectively. M_w is the mass of water in the filter paper, and M_f is the mass of the dry filter paper. The suction values were determined using the calibration curves in Figure 2.

$$W_f = \frac{M_w}{M_f} \times 100 \tag{10}$$

2.2.4 Triaxial testing

The triaxial test was conducted according to the standard [47]. The specimen measured 300 mm in height and 150 mm in diameter with a diameter/height ratio of 1.2. The soil specimens were prepared within the range of (11 – 12) kg. After oven drying, a sufficient mass of soil (plus 10 %) and water were mixed to produce a specimen. The water volumes were based on Proctor test results. Vibro-compaction required five equal layers, each with a duration of five minutes. An extruder removed the specimen from the mould, which was then trimmed to

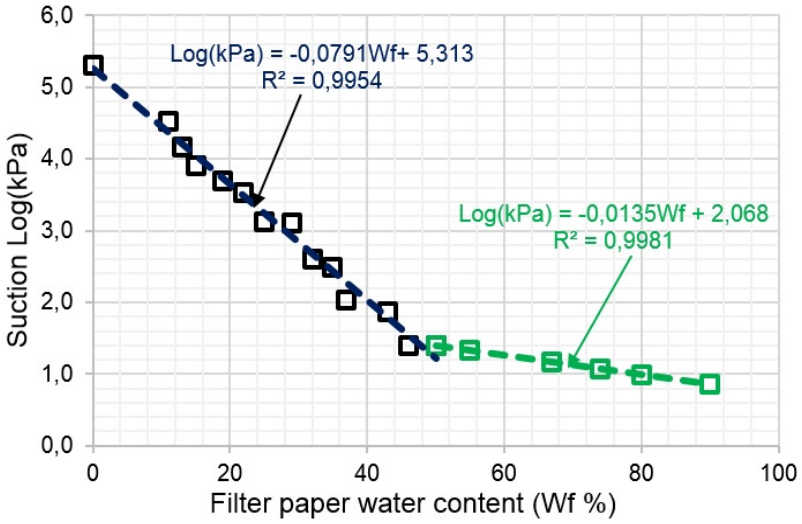

Figure 2: Whatman No. 42 filter paper calibration curve [4].

Figure 3: Triaxial testing apparatus.

the required dimensions and weighed. Figure 3 shows the equipment for triaxial testing. The consolidated undrained (CU) triaxial test measured the shear strength characteristics of the prepared soil specimens. A set of three static triaxial tests provided data for each density/water content condition. The confining pressures for these three tests are 50, 100, and 150 kPa.

3 Results and discussion

3.1 Material properties

Table 3 shows the material properties. The particle size analysis revealed that the fine content is not uniform for all tested soils. WES exhibited the highest amount of fine content among other samples, followed by WIS, BFS and BES. More than 50 % of tested soils passed the No 200 (0.075mm) sieve. BES showed a fine content of 45.14 %, higher than the sand content. The tested soils exhibited a liquid limit (LL) of (40.29 – 69.34) % and a plastic limit (PL) of (19.23 – 49.87) %. BFS, WIS and WES exhibited high plasticity and BES low plasticity. Figures 25 and 26 in Appendix 7 show the grain size distribution curves and the plasticity chart of four soil samples. Table 4 in Appendix 1 outlines the swelling potential test results. The tested soils portrayed a free swell index range of (35.81 – 116.60) %, with a free swell ratio of 1.17 – 2.20. The results confirmed that BFS, WIS and WES exhibited high plasticity and BES low plasticity and the swelling behaviour of tested soils. Table 5 in Appendix 1 shows the compaction characteristics of tested soil samples. The variability of fine-grained soils in tested samples significantly influenced the values of compaction features [48]. The OWC and γ_{dmax} values ranged from (17.20 – 26.10) % and (16.30 – 19.60) kN/m^3, respectively. The results are consistent with the findings reported by [49, 50, 51, 52, 53, 54, 55].

Table 3: Material properties.

Soils	Liquid limit (%)	Plasticity index (%)	Clay (%)	Ac*	Silt (%)	Fine content (%)	Sand (%)	Gravel (%)	Specific Gravity (Gs)	USCS
BFS	58.98	36.82	30.40	1.21	29.11	59.51	29.39	10.09	2.64	CH
WIS	63.78	42.48	34.03	1.25	33.49	67.52	26.80	4.85	2.73	CH
WES	69.45	49.87	40.00	1.25	33.00	73.00	23.50	2.56	2.73	CH
BES	40.29	19.23	17.11	1.12	28.03	45.14	43.76	11.10	2.55	CL

*Ac: Activity of clay

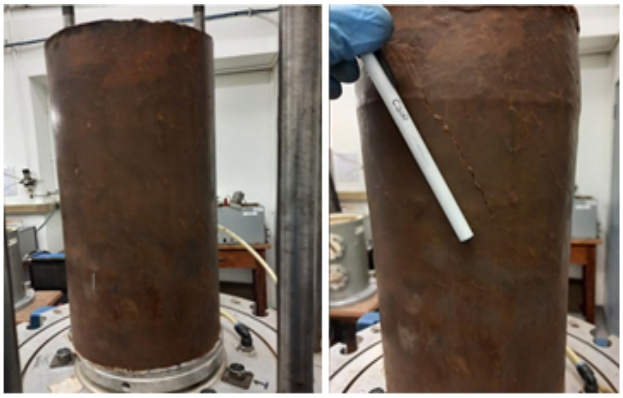

Figure 4: Typical specimen before and after failure.

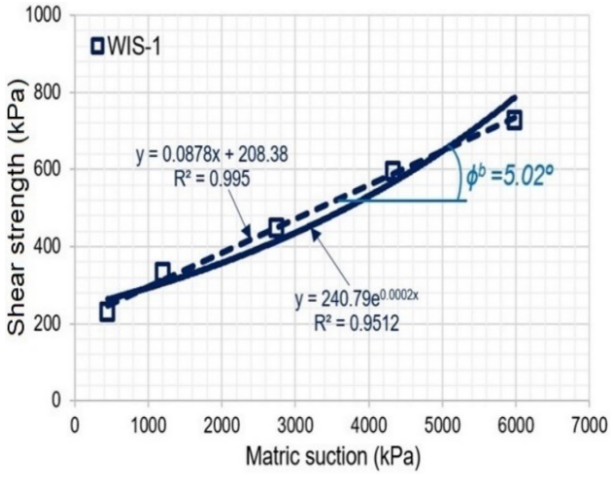

Figure 5: Unsaturated failure envelope for WIS

3.2 X-ray diffraction

Table 6 in Appendix 1 summarises the X-ray diffraction results of studied soil samples. The results show that the smectite is the prevailing clay mineral. A small amount of illite and trace illite was observed. Silica and feldspar (plagioclase, K-feldspar) are the predominant non-clay minerals. A slight amount and trace of calcite appeared in soil samples. The results agree with the study published by [4, 5]. The significant amount of smectite can explain the swelling characteristics of soil samples, and the results are in line with the swelling potential analysis report.

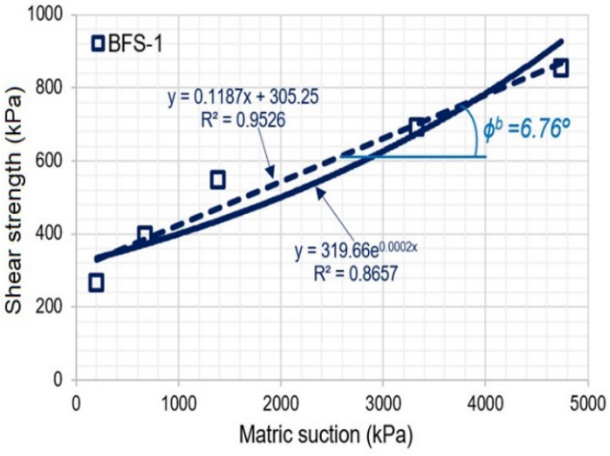

Figure 6 Unsaturated failure envelope for BFS.

3.3 Soil suction test

The suction values were estimated at different water content using the Whatman No 42 type filter paper technique (FPT) at the initial state. The principle of FPT is to measure the suction indirectly by relating the water absorbed by the specified filter paper with suction through a calibration curve. Matric suction and total suction were measured from soil specimens, and osmotic suction was obtained as the variation between total and matric suction. Table 7 in Appendix 2 shows the suction test results. The tested soils displayed a total suction of (110 – 9926) kPa and a matric suction of (80 – 7694) kPa. The results indicated that the soil suction range values agree with a similar study conducted by [56, 57, 58, 59]. Figures 27 through 30 in Appendix 7 describe the soil water characteristic curves (SWCCs) for soil samples BFS,

WIS, WES and BES, respectively. The air entry value (AEV) of tested soils is summarised in Table 7 and shows the matric suction values at AEV ranging from (6 – 16.13) kPa. The results align with the findings reported by [45, 54].

3.4 Triaxial testing results

The consolidated undrained triaxial tests were performed on prepared unsaturated soil specimens at different water content. Figure 4 shows a typical specimen before and after shear failure. The extended Mohr–Coulomb shear strength criterion for unsaturated soils provides the saturated shear strength characteristics (c‘, ϕ‘) and the matric suction angle ϕ^b. In this study, ϕ^b is measured as the slope between the shear strength and matric suction curve denoted as an unsaturated soil failure envelope. Figure 5 shows the unsaturated failure envelope for sample WIS with ϕ^b = 5.02°, and Figure 6 portrays the unsaturated failure envelope for sample BFS with ϕ^b = 6.76°. The triaxial test results are presented in Table 8, Appendix 2. The reported unsaturated shear strength (τ_u) values range from (196 – 1512) kPa, and the saturated shear strength (τ_s) values range from (154 – 941) kPa. τ_u values were found to be 1.05 – 1.76 times higher than (τ_s) values due to the contribution of matric suction to the shear strength. The studied soils describe a friction angle (ϕ‘) of (25 – 53)º, a matric suction angle (ϕ^b) of (2.67 – 10)º and a cohesion (c‘) of (45 – 78) kPa. The values of ϕ‘ and ϕ^b are in line with the research works by [60, 61, 62, 4, 9, 79] reporting that ϕ^b is smaller than ϕ‘ ($\phi^b < \phi$‘).

3.5 Shear strength parameters’ response to geotechnical index properties and soil mineralogy

The shear strength parameters’ response to geotechnical index properties and soil mineralogy was investigated in this section, based on experimental data obtained from tested soil samples. The shear strength parameters include the saturated friction angle (ϕ'), the matric suction angle (ϕ^b) and soil cohesion (c‘). The degree of correlation between the dependent variables was interpreted according to Table 9 in Appendix 3 proposed by [63].

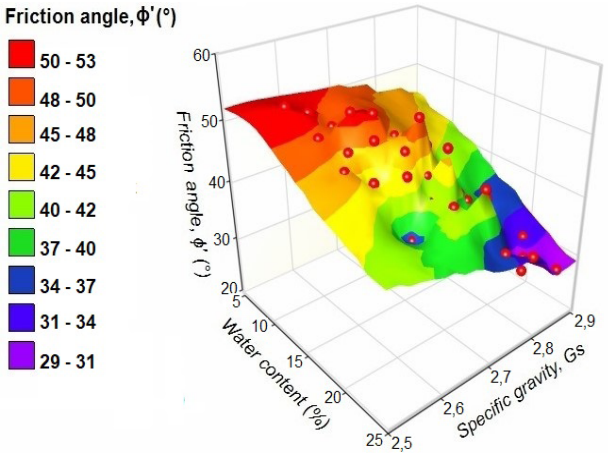

Figure 7: 3D relationship of (ϕ‘) dependence on W (%) and Gs.

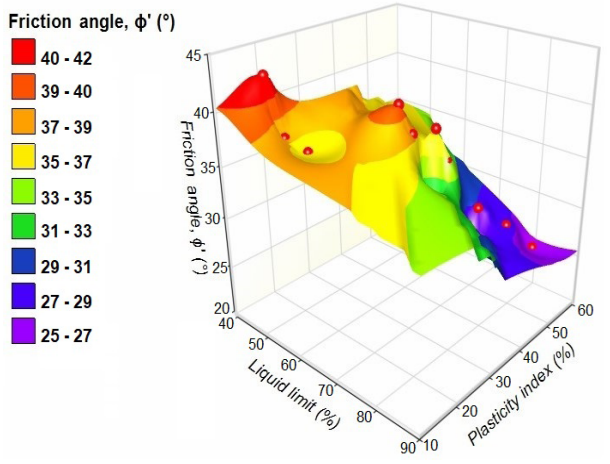

Figure 8: 3D relationship of (ϕ‘) dependence on liquid limit and plasticity index.

3.5.1 Relationships between friction angle ϕ' and water content, specific gravity, liquid limit and plasticity index

Figures 7 and 8 depict the relationship between (ϕ') and soil parameters: water content, Gs, LL and PI. Figure 7 illustrates the surface plot of (ϕ'), water content and Gs. ϕ' decreases as Gs increases, displaying a strong correlation (R^2=0.72) with Gs as given in Equation 11 in Table 10, Appendix 3. The correlation highlights the influence of Gs on ϕ', a result consistent with the findings published by [64]. The ϕ' of tested soils decreases as water content increases, following a strong correlation (R^2=0.71) provided in Equation 12 in Table 10, Appendix 3. The increment in water content within the soil material reduces the resistance to interlocking of soil particles, aligning with other studies published by [14, 15, 65, 66, 67] emphasising on the strong dependency of water content

on ϕ'. Figure 8 exhibits the surface plot of ϕ', LL and PI. ϕ' decreases with the increasing of LL, displaying a moderate exponential correlation (R^2=0.68) described in Equation 13 in Table 10, Appendix 3. Similarly, ϕ' decreases as the PI of the soil sample increases, showing a moderate relationship (R^2=0.64) described in Equation 14, Table 10, Appendix 3. The trend can be attributed to the reduction in resistance to the interlocking of soil particles with the increase of Atterberg limits due to water content. The results correspond with the findings reported by [19, 68, 69], indicating a moderate influence of Atterberg limits on the friction angle.

Figures 31 to 33 in Appendix 8 compare the relationships between the friction angle (ϕ') and water content, specific gravity and liquid limit from this study with the results from other researchers such as [14, 15, 65, 67, 76, 68]. Similar trends are observed from the data graphs (Figures 31–33), the friction angle decreases as water content, specific gravity, and liquid limit increase. The marginal discrepancies observed stem from the soil material's variability and the limited number of soil specimens utilised by other researchers.

3.5.2 Relationships between friction angle ϕ' and fine content, clay content, dry unit weight and void ratio

Figures 9 and 10 present a three-dimensional representation of the relationship between ϕ', fine content, clay content, dry unit weight (γ_d) and void ratio. Figure 9 displays a three-dimensional graph of ϕ', fine content and clay content. ϕ' decreases as the fine content increases in soil material, portraying a strong correlation (R^2=0.72) as provided in Equation 15 in Table 10, Appendix 3. The friction angle decreases with the increase in clay content within the soil, exhibiting a strong correlation (R^2=0.74) described in Equation 16 in Table 10, Appendix 3. The reaction of fine-grained particles with water reduces the resistance to the interlocking of soil particles, aligning with studies reported by [70, 71]. Figure 10 portrays the surface plot of ϕ', dry unit weight and void ratio. The ϕ' angle increases with an increase in dry unit weight, showing a moderate correlation (R^2=0.62) with dry unit weight as described in the exponential Equation 17 in Table 10, Appendix 3. The finding agrees with studies reported by [14, 72, 15] on the shear strength of expansive soils. ϕ' of soil material decreases as the void ratio increases, exhibiting a moderate correlation (R^2=0.70) with the void ratio described in Equation 18 in Table 10, Appendix 3. The result aligns with research published by [24, 17] on the impact of soil fabric on shear strength.

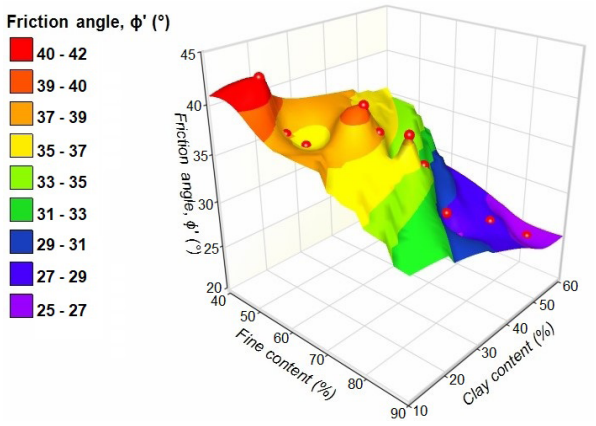

Figure 9: 3D relationship of (ϕ') dependence on fine content (%) and clay content (%).

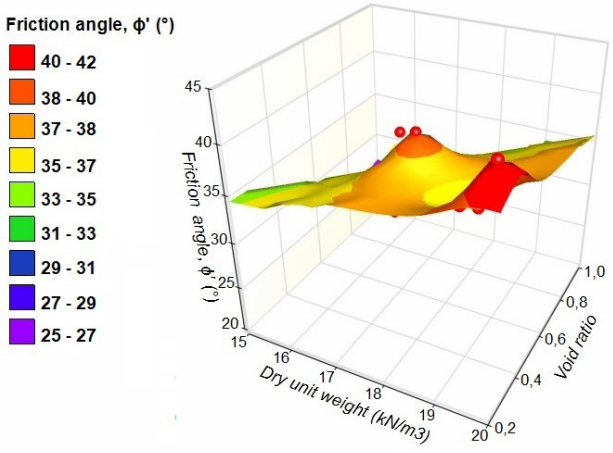

Figure 10: 3D relationship of (ϕ') dependence on dry unit weight and void ratio.

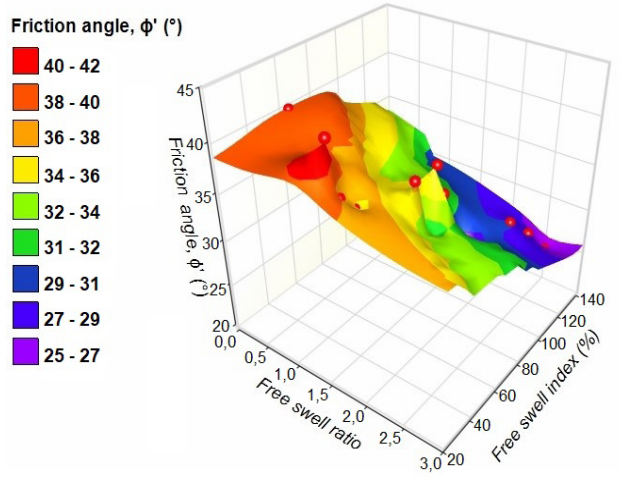

Figure 11: 3D relationship of (ϕ') dependence on FSR and FSI (%).

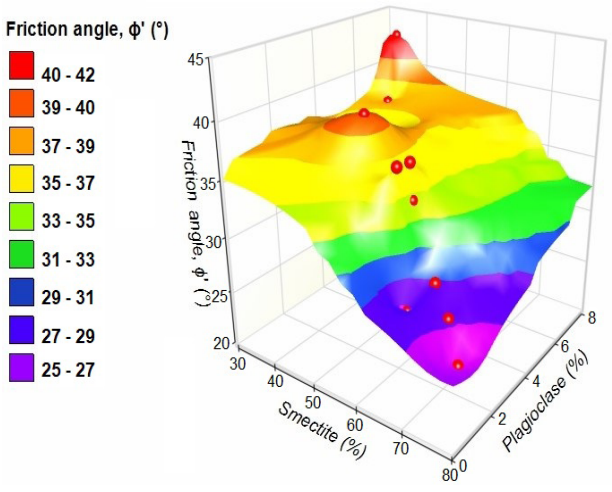

Figure 12: 3D relationship of (ϕ‘) dependence on smectite (%) and plagioclase (%).

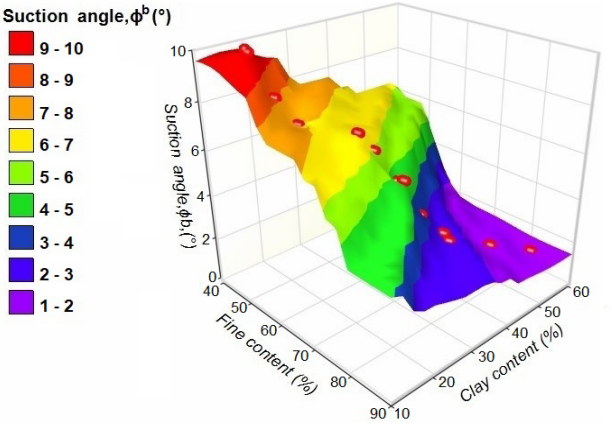

Figure 13: 3D relationship of (ϕ^b) dependence on fine content (%) and clay content (%).

3.5.3 Relationships between friction angle ϕ' and free swell ratio, free swell index, smectite content and plagioclase content

Figures 11 and 12 portray a three-dimensional description of the correlation between ϕ' and soil characteristics such as free swell ratio (FSR), free swell index (FSI), smectite content and plagioclase content. Figure 11 illustrates the relationship among ϕ', FSR and FSI. The friction angle decreases as FSR increases. The exponential Equation 19 in Table 10, Appendix 3, demonstrates a strong correlation (R^2=0.74) between ϕ' and FSR. ϕ' decreases with an increase in FSI of the tested soil, as indicated by the strong correlation (R^2=0.70) described in Equation 20 in Table 10, Appendix 3. ϕ' decreases with a higher swelling potential, aligning with the findings from reports

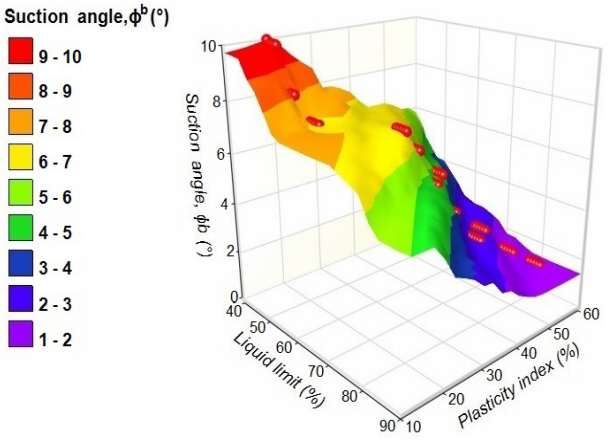

Figure 14: 3D relationship of (ϕ^b) dependence on liquid limit (%) and plasticity index (%).

by [16, 73] for similar soils. Figure 12 shows a surface plot of ϕ', smectite content and plagioclase content. As the smectite content increases, ϕ' decreases with a moderate correlation (R^2=0.61) as described in Equation 21 in Table 10, Appendix 3. This indicates that clay mineral (smectite) content influences ϕ'. The results are in line with research published by [30, 31], demonstrating the decrease in ϕ' with the increment of clay mineral quantity. On the other hand, ϕ' increases with the increase in plagioclase content and portrays a moderate correlation (R^2=0.53) described in Equation 22 in Table 10, Appendix 3. The trend can be attributed to the presence of plagioclase, enhancing the resistance to interlocking of soil particles. Figure 37 in Appendix 4 describes the correlation diagram of ϕ‘ and the soil properties.

3.5.4 Correlations between matric suction angle ϕ^b and fine content, clay content, liquid limit and plasticity index

Figures 13 and 14 describe the correlation between the matric suction angle (ϕ^b) and the soil features such as fine content, clay content, LL and PI. Figure 13 presents a surface plot of ϕ^b, fine content and clay content. ϕ^b decreases as the fine content increases and exhibits a strong correlation (R^2=0.92) given in Equation 23 in Table 11, Appendix 3. ϕ^b decreases with an increase in clay content and demonstrates a strong correlation (R^2=0.92) described in Equation 24 in Table 11, Appendix 3. The trend corroborates other studies reported by [30, 31] for similar expansive soils. Figure 14 shows the correlation between ϕ^b, LL and PI. ϕ^b decreases as the LL and PI increase. ϕ^b demonstrates a strong correlations with R^2=0.93 for LL and R^2=0.92 for PI as given in Equations

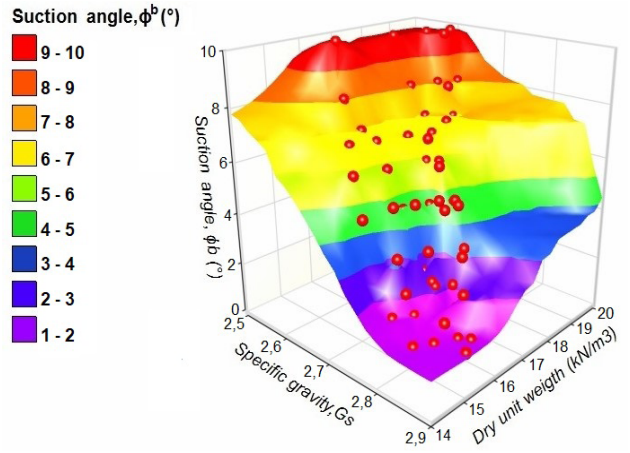

Figure 15: 3D relationship of (ϕ^b) dependence on Gs and dry unit weight.

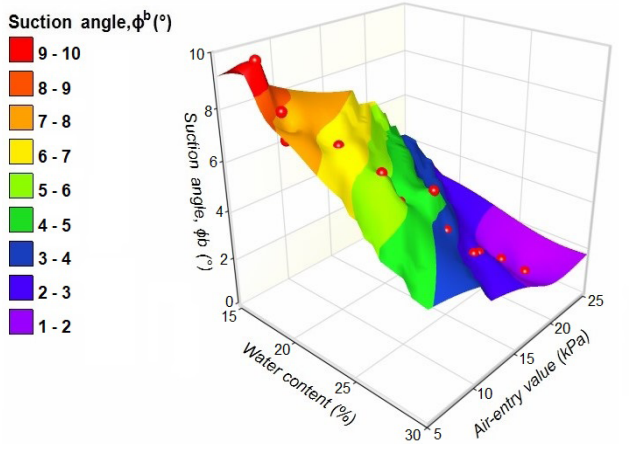

Figure 16: 3D relationship of (ϕ^b) dependence on water content (%) and air entry value.

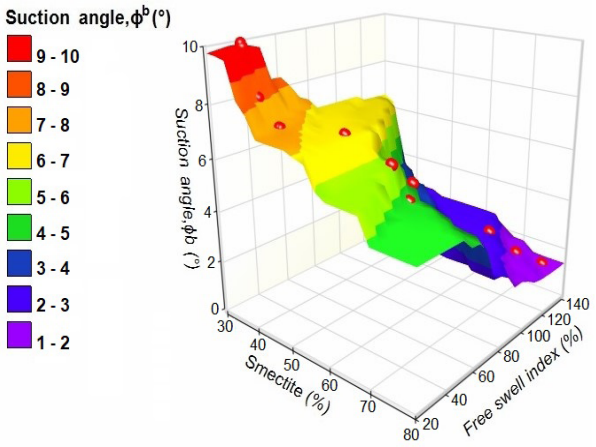

Figure 17: 3D relationship of (ϕ^b) dependence on smectite (%) and FSI (%)

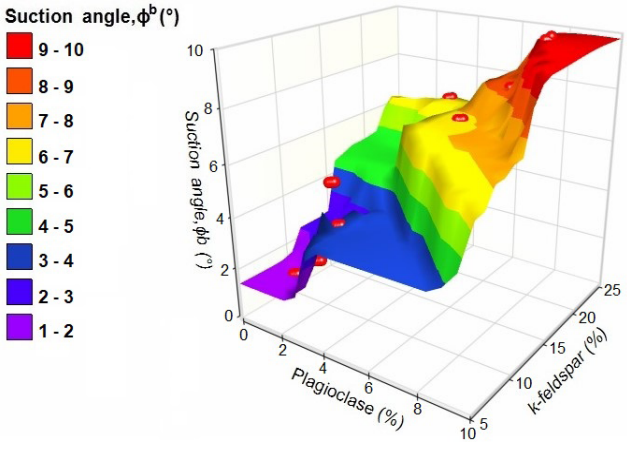

Figure 18: 3D relationship of (ϕ^b) dependence on plagioclase (%) and K-feldspar (%)

25 and 26 in Appendix 3, respectively. The findings are in line with the results reported by [19, 15], highlighting the influence of Atterberg limits on the shear strength of unsaturated soils.

3.5.5 Correlations between matric suction angle ϕ^b and specific gravity, dry unit weight, water content and air entry value

Figures 15 and 16 describe the relationship between ϕ^b and soil parameters: Gs, γ_d, water content, and air entry value. Figure 15 illustrates the surface plot of ϕ^b, Gs, and γ_d. ϕ^b decreases as Gs increases, showing a strong correlation (R^2=0.88) with Gs, as described in Equation 27 in Table 11, Appendix 3. This trend can be justified by the increase in Gs with the augmentation of clay content, leading to an increment of negative pore pressure and a subsequent decrease in ϕ^b. ϕ^b increases with an increase in γ_d of the soil material, showing a strong correlation (R^2=0.81) with γ_d as given in Equation 28 in Table 11, Appendix 3. These results are consistent with studies reported by [21, 14, 15] on the shear strength of unsaturated soils. Figure 16 describes a surface plot of ϕ^b, water content, and AEV. ϕ^b decreases as water content increases, exhibiting a strong correlation (R^2=0.88) with water content as given in Equation 29 in Table 11, Appendix 3. The results align with research published by [14, 15, 16], showing a decrease in the shear strength of expansive soils with the increase of water content. ϕ^b decreases with an increase in AEV, showing a very strong correlation (R^2=0.92) with AEV as described in Equation 30 in Table 11, Appendix 3. The trend is in line with the results published by [27, 28, 29], reporting the influence of AEV on unsaturated shear strength.

3.5.6 Correlations between matric suction angle ϕ^b and smectite content, free swell index, plagioclase content and K-feldspar content

Figures 17 and 18 illustrate the three-dimensional relationship between ϕ^b and smectite content, FSI, plagioclase content and K-feldspar content. Figure 17 depicts the surface plot of ϕ^b, smectite content, and FSI. ϕ^b decreases as FSI increases, showing a very strong correlation (R^2=0.93) with FSI as described in Equation 31 in Table 11, Appendix 3. The decrease in shear strength with the increment of swelling potential aligns with findings from reports by [74, 16, 73] on unsaturated shear strength. ϕ^b decreases with an increase in smectite content, showing a strong correlation (R^2=0.79) with smectite content according to Equation 32 in Table 11, Appendix 3. The proportion of smectite significantly impacts the shear strength of expansive soils, and the results are consistent with studies reported by [20, 30, 31] on similar soils. Figure 18 presents a surface plot of ϕ^b, plagioclase content, and K-feldspar content. ϕ^b increases with higher plagioclase content in soil material, showing a moderate correlation (R^2=0.67) with plagioclase content described in Equation 33 in Table 11, Appendix 3. ϕ^b increases with higher K-feldspar content, displaying a moderate correlation (R^2=0.66) with K-feldspar as outlined in Equation 34 in Table 11, Appendix 3. Figure 38 in Appendix 5 describes the correlation diagram of ϕ^b and the soil properties.

3.5.7 Relationships between effective cohesion c‘ and water content, specific gravity, liquid limit and plasticity index

Figures 19 and 20 provide a three-dimensional description of the correlation between c‘ and soil features such as water content, Gs, LL and PI. Figure 19 presents a surface plot of c‘, water content, and Gs. c‘ decreases as water content increases and demonstrates a strong correlation (R^2=0.73) as given in Equation 35 in Table 12, Appendix 4. This trend can be explained by the decrease in intermolecular bonds between the water and grain particles with the increase in water content. The observation is in line with the reports published by [13, 14, 75, 66, 17], presenting a strong dependency of c‘ on water content. c‘ decreases with an increase in Gs and exhibits a strong correlation (R^2=0.71) as described in Equation 36 in Table 12, Appendix 4. The finding aligns with the study reported by [64] on variability in the geotechnical properties of clay soils. It appeared that Gs and water content influence soil cohesion. Figure 20 displays the surface plot of c‘, LL, and

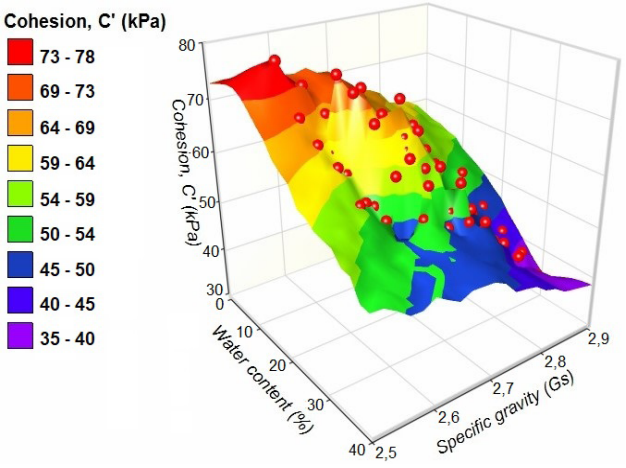

Figure 19: 3D relationship of (c') dependence on water content (%) and specific gravity.

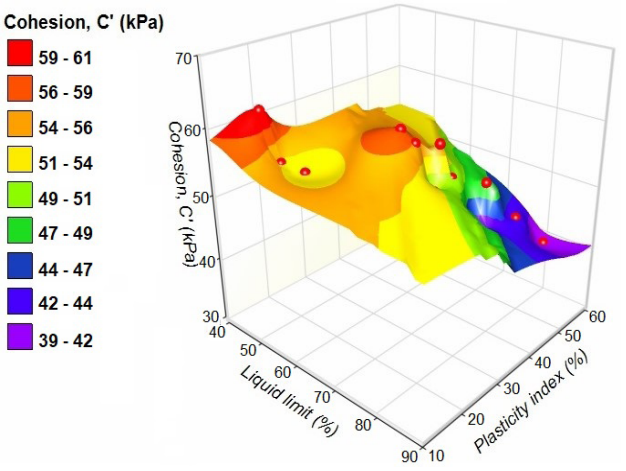

Figure 20: 3D relationship of (c') dependence on liquid limit (%) and plasticity index (%).

PI. The surface plot illustrates a reduction in c‘ with the increase in LL, and PI. The correlation between c‘, LL and PI demonstrates a moderate correlation with (R^2=0.61) for LL and (R^2=0.56) for PI as described in Equations 37 and 38, respectively, in Table 12, Appendix 4. The trend can be attributed to the fact that LL and PI increase with the increment of water and reduce the intermolecular bond between the adsorbed water surrounding each grain in soil material. The LL and PI influence the magnitude of soil cohesion. The findings align with the results reported by [69, 68, 76] depicting the influence of Atterberg limits on soil cohesion.

Figures 34 to 36 in Appendix 8 compare the relationships between the effective cohesion (c‘) and water content, specific gravity and liquid limit from this

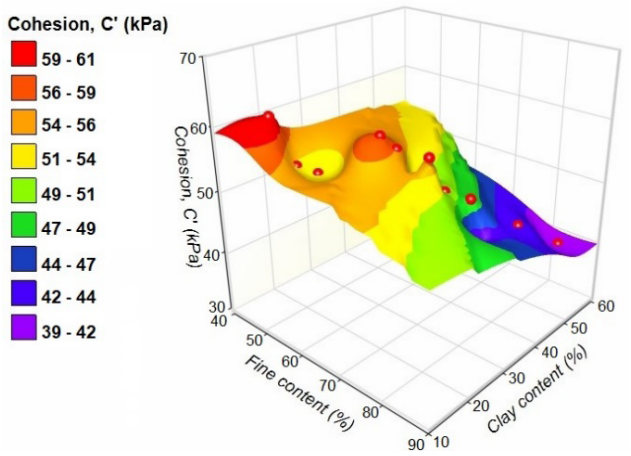

Figure 21: 3D relationship of (c') dependence on fine content (%) and clay content (%).

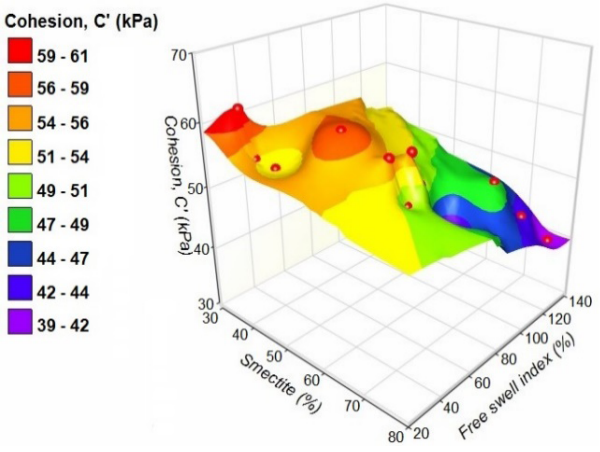

Figure 23: 3D relationship of (c') dependence on smectite (%) and free swell index (%).

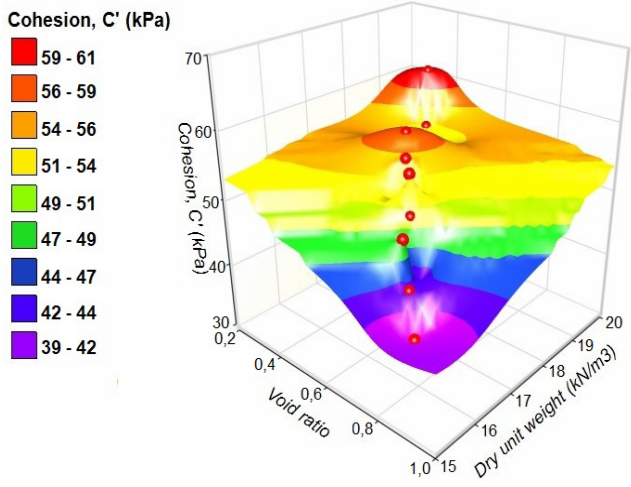

Figure 22: 3D relationship of (c') dependence on dry unit weight and void ratio.

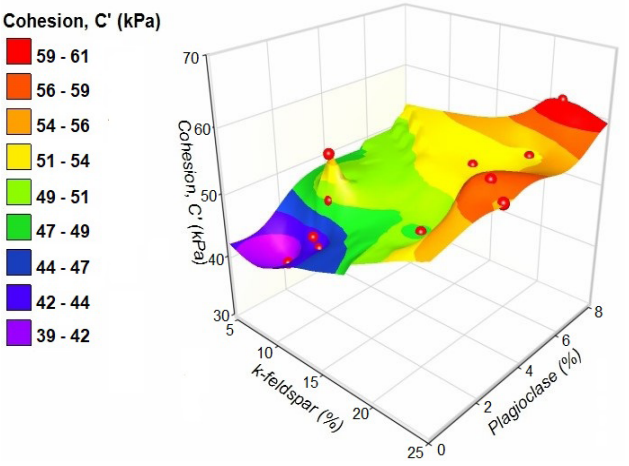

Figure 24: 3D relationship of (c') dependence on K-feldspar (%) and plagioclase (%).

study with the results from other scholars like [14, 15, 65, 67, 76, 68]. Similar trends are observed from the data graphs (Figures 34 to 36), the friction angle decreases as water content, specific gravity, and liquid limit increase. The marginal discrepancies observed stem from the soil material's variability and the limited number of soil specimens utilised by other researchers.

3.5.8 Relationships between effective cohesion c' and fine content, clay content, void ratio and dry unit weight

Figures 21 and 22 describe the correlation between c' and soil features such as fine content, clay content, void ratio, and γ_d. Figure 21 presents the surface plot of c', fine content, and clay content. There is a tendency for c' to decrease when the fine content increases. c' shows a moderate correlation (R^2=0.68) with fine content described in Equation 39 in Table 12, Appendix 4. Similarly, c' tends to decrease as the clay content in soil grows. c' portrays a strong correlation (R^2=0.71) with clay content as given in Equation 40 in Table 12, Appendix 4. The trend can be explained by the fact that clays and silts react with water, change sizes and reduce the intermolecular bond between the adsorbed water surrounding each grain. The findings agree with the trends observed in the studies published by [20, 30] on the shear strength of swelling soils. Figure 22 shows the surface graph of c', void ratio and γ_d. c' decreases as the void ratio increases, indicating a moderate correlation (R^2=0.64) described in Equation 41 in Table 12, Appendix 4. The trend stems from the

presence of significant amounts of clays and silts that lead to more voids and less particle-to-particle contact. Consequently, the increase in the void ratio reduces soil cohesion. The observation agrees with other research studies reported by [24, 71, 17, 76] on the shear strength properties of soil materials. c‘ increases when γ_d increases and exhibits a moderate correlation (R^2=0.54) described in Equation 42 in Table 12, Appendix 4. The increment of γ_d enhances the intermolecular bond between the adsorbed water surrounding each grain in the soil material justified the trend. The finding concurs with the studies published by [14, 15, 76] on similar soils. The void ratio and dry unit weight influence the soil cohesion.

3.5.9 Relationships between effective cohesion c‘ and smectite content, free swell index, K-feldspar content and plagioclase content

Figures 23 and 24 describe the relationship between c‘ and soil parameters: smectite content, FSI, K-feldspar content, and plagioclase content. Figure 23 portrays the surface plot of c‘, smectite content and FSI. c‘ decreases with the growth of smectite content and exhibits a moderate correlation (R^2= 0.52) with the smectite content described in Equation 43 in Table 12, Appendix 4. The results align with the studies published by [20, 31], indicating that c‘ decreases with the increment of clay minerals within the soil. Another study reported by [30] stated that c‘ reduces when the quantity of clay minerals increases. Similarly, c‘ decreases when the FSI of soil increases and displays a moderate correlation (R^2=0.62) described in Equation 44 in Table 12, Appendix 4. The trend is consistent with other investigations reported by [16, 73] for similar expansive soils. Figure 24 shows the surface graph of c‘, K-feldspar content, and plagioclase content. c‘ increases when K-feldspar content increases and shows a moderate correlation (R^2=0.53) with K-feldspar content, as given in Equation 45 in Table 12, Appendix 4. c‘ increases when the plagioclase content grows and portrays a moderate correlation (R^2=0.51) with plagioclase content described in Equation 46 in Table 12, Appendix 4. Figure 39 in Appendix 5 describes the correlation diagram of c‘ and the soil properties.

4 Concluding remarks

The research focused on assessing the influences of soil index properties, swelling parameters, and soil mineralogy on unsaturated shear strength parameters of compacted expansive soils. Four soil samples were collected across the study areas and divided into twenty specimens with different water content. The laboratory investigations provided the soil index properties, swelling potential, compaction characteristics, soil suction, and shear strength characteristics of tested soil samples.

The matric suction angle ϕ^b is majorly influenced by the soil properties such as the fine content, clay fraction, liquid limit, plasticity index, air entry value, free swell index, smectite content, water content, dry unit weight, and specific gravity. This can be explained by the significant amount of fine content and smectite content in soil samples. ϕ^b significantly influences the unsaturated shear strength of the soil sample. ϕ^b bears a moderate correlation with the plagioclase and K-feldspar contents. This can be justified by the presence of a marginal fraction of non-clay minerals in soil samples. ϕ^b increases when the dry unit weight, plagioclase content, and K-feldspar content increase. On the other hand, ϕ^b decreases as the fine content, clay content, liquid limit, plasticity index, specific gravity, water content, smectite content, and free swell index increase.

The friction angle $\phi‘$ exhibits a strong correlation with water content, specific gravity, fine content, clay content, void ratio, free swell index, and free swell ratio. $\phi‘$ bears a moderate correlation with plastic limit, liquid limit, dry unit weight, clay mineral fraction (smectite) and a non-clay mineral fraction (plagioclase). This can be justified by the fact that the soil fabric plays an essential role in the mechanical behaviour of soils. $\phi‘$ increases when the dry unit weight and the plagioclase content increase. Nonetheless, $\phi‘$ decreases when the water content, specific gravity, free swell index, free swell ratio, clay fraction, liquid limit, plasticity index, fine content, void ratio and smectite content increase in the soil material.

The effective cohesion c‘ is majorly influenced by soil properties such as water content, specific gravity, and clay fraction. c‘ bears a moderate correlation with the liquid limit, plasticity index, fine content, void ratio, dry unit weight, smectite content, free swell index, K-feldspar, and plagioclase contents. The soil fabric, mineral composition and stress state influence the soil behaviour. c‘ increases when the dry unit weight, plagioclase content and K-feldspar content increase. On the other hand, c‘ decreases as the water content, specific gravity, liquid limit, plasticity index, fine content, clay fraction, void ratio, smectite content and free swell index increase.

The findings provide a good insight into the behaviour of compacted expansive soils and contribute to improving the application of geotechnical modelling of the problematic expansive soils. Further investigation should

be conducted on the shear strength response to other soil index properties not mentioned in this study.

Acknowledgements

The authors thank the Central University of Technology, Free State, for sponsoring this research project.

List of abbreviations

ϕ'	Angle of internal friction of effective normal stress
ϕ^b	Matric suction angle
c‘	Effective cohesion of soil material
γ_d	Dry unit weight
γ_{dmax}	Maximum dry unit weight
χ	Bishop parameter
τ_s	Saturated shear strength
τ_u	Unsaturated shear strength
σ_n	Total normal stress
θ	Volumetric water content
θ_r	Residual volumetric water content
θ_s	Saturated volumetric water content
CH	High plastic clay
CL	Low plastic clay
Gs	Specific gravity
Sr	Degree of saturation
k	Fitting parameter
R^2	Coefficient of determination
u_a	Pore air pressure
u_w	Pore water pressure
$u_a - u_w$	Matric suction
P_{at}	Atmospheric pressure
AEV	Air entry value
BES	Bethlehem soil
BFS	Bloemfontein soil
FPT	Filter paper technique
FSI	Free swell index
FSR	Free swell ratio
GPS	Global positioning system
LL	Liquid limit
OWC	Optimum water content
PI	Plasticity index
SWCC	Soil water characteristic curve
USCS	Unified soil classification system
WES	Welkom Soil
WIS	Winburg Soil
XRD	X-ray diffraction

References

[1] Lal, R. Ed., 2006. *Encyclopedia of soil science* (No. 11). CRC Press.

[2] Jones, L.D. and Jefferson, I., 2012. Expansive soils, pp. 413-441. *Institute of Civil Engineers* Publishing, London.

[3] Fondjo, A.A., 2018. Characterization of swelling stress and soil moisture deficiency relationship for expansive unsaturated soils. Master Dissertation, Department of Civil Engineering, Central University of Technology, Free State.

[4] Fondjo, A.A., 2024. Characterization of the shear stress properties of compacted unsaturated heaving soils. *Doctorate Thesis, Department of Civil Engineering, Central University of Technology, Free State*.

[5] Fondjo, A.A. and Theron, E., 2020. Assessment of mineral composition of heaving soils using some soil properties. *Civil Engineering and Architecture*, Vol. 8, No. 4, pp. 619 - 631. DOI: 10.13189/cea.2020.080425

[6] Abeb, A.A. and Vermeer, P.A., 2009. Numerical simulation of unsaturated soil behaviour. *International Journal of Computer Applications in Technology*, Vol. 34, No. 1, pp. 2-12. DOI: 10.1504/IJCAT.2009.022697

[7] Fondjo, A.A., Theron, E. and Ray, R.P., 2021. Models for predicting the suction of heaving compacted soils using geotechnical properties.*14th Baltic Sea geotechnical conference 2021 Helsinki, Finlande*. IOP Conference Series: Earth and Environmental Science, Vol. 727. DOI: 10.1088/1755-1315/727/1/012016

[8] Blight, G.E., 2013. *Unsaturated soil mechanics in geotechnical practice*. CRC Press.

[9] Fondjo, A.A., Theron, E. and Ray, R.P., 2023. Evaluation of the Unsaturated Shear Strength Parameters of Compacted, Heaving Soil Using Geotechnical Properties. In *8th International Conference on Unsaturated Soils 2023, Milos, Greece.* In *E3S Web of Conferences* 382: 02002. DOI: 10.1051/e3sconf/202338202002

[10] Sailie, E.L. and Bucher, F., 1984. Shear strength properties of tropical black clays. In *Regional conference for Africa.* Vol. 8, pp. 99-103.

[11] Calabresi, G. and Scarpelli, G., 1985. Effects of swelling caused by unloading in over consolidated clays. In *International conference on soil mechanics and foundation engineering.* Vol. 11, pp. 411-414.

[12] Toll, D.G., 1990. A framework for unsaturated soil behaviour. *Géotechnique*, Vol. 40, No.1, pp. 31-44. DOI: 10.1680/geot.1990.40.1.31

[13] Stark, T.D. and Duncan, J.M., 1992. Mechanisms of strength loss in stiff clays. *Journal of Geotechnical Engineering*, Vol. 118, No. 6, pp. 976-977.

[14] Chen, Y., Zhao, J. and Hu, X.H., 2012. Research on the shear strength properties of expansive soils. *Applied Mechanics and Materials*, Vol. 256-259, pp. 287-292. DOI: 10.4028/www.scientific.net/amm

[15] Chowdhury, R.H., 2013. *Shear strength properties of compacted expansive soils*. Master dissertation, University of Regina.

[16] Domitrović, D. and Zelić, B.K., 2013. The relationship between swelling and shear strength properties of bentonites. In *Proceedings of the 18th International Conference on Soil Mechanics and Geotechnical Engineering, Paris*. pp. 219-222.

[17] Wang, L.C., Long, W. and Gao, S.J., 2014. Effect of moisture content, void ratio and compacted sand content on the shear strength of remolded unsaturated clay. *Electronic Journal of Geotechnical Engineering*, Vol. 19, pp. 4413-4426.

[18] Vanapalli, S.K. and Fredlund, D.G., 2000. Comparison of empirical procedures to predict the shear strength of unsaturated soils using the soil-water characteristic curve. *Advances in unsaturated geotechnics*, Vol. 99, pp.195-209.

[19] Garven, E.A. and Vanapalli, S.K., 2006. Evaluation of empirical procedures for predicting the shear strength of unsaturated soils. *4th International Conference on Unsaturated Soils, April 2-6, 2006, Arizona, United States*.

[20] Escario, V., 1980. Suction controlled penetration and shear tests. In *Expansive Soils*. *Proc.4th international conference on Expansive soils,* ASCE, pp. 781-797.

[21] Escario, V., Juca, J.F.T. and Coppe, M.S., 1989. Strength and deformation of partly saturated soils. In *Congrès international de mécanique des sols et des travaux de fondations.* Vol. 12, pp. 43-46.

[22] Casagrande, A. and Hirschfeld, R.C., 1960. Stress-deformation and strength characteristics of a clay compacted to a constant dry unit weight, *In Research Conference on Shear Strength of Cohesive Soils,* ASCE, pp. 359-417.

[23] Zewdie, A., 2004. *Investigation in to shear strength characteristics of expansive soil of Ethiopia*. Doctoral dissertation, Addis Ababa University.

[24] Warkentin, B.P. and Yong, R.N., 1962. Shear strength of montmorillonite and kaolinite related to interparticle forces. In *Proceeding the 9th National Conference on Clays and Clay Minerals*, pp. 210-218.

[25] Khalili, N. and Khabbaz, M.H., 1998. A unique relationship for χ for the determination of the shear strength of unsaturated soils. *Géotechnique*, Vol. 48, No. 5, pp. 681-687.

[26] Gan, J.K.M., Fredlund, D.G. and Rahardjo, H., 1988. Determination of the shear strength parameters of an unsaturated soil using the direct shear test. *Canadian Geotechnical Journal*, Vol. 25, No. 3, pp. 500-510. DOI: 10.1139/t88-055

[27] Vanapalli, S.K., Fredlund, D.G., Pufahl, D.E. and Clifton, A.W., 1996. Model for the prediction of shear strength with respect to soil suction. *Canadian geotechnical journal*, Vol. 33, No. 3, pp. 379-392.

[28] Tekinsoy, M.A., Kayadelen, C., Keskin, M.S. and Söylemez, M., 2004. An equation for predicting shear strength envelope with respect to matric suction. *Computers and Geotechnics*, Vol. 31, No. 7, pp. 589-593.

[29] Guan, G.S., Rahardjo, H. and Choon, L.E., 2010. Shear strength equations for unsaturated soil under drying and wetting. *Journal of Geotechnical and Geoenvironmental Engineering*, Vol. 136, No.4, pp. 594-606.

[30] Morrow, C.A., Shi, L.Q. and Byerlee, J.D., 1984. Permeability of fault gouge under confining pressure and shear stress. *Journal of Geophysical Research: Solid Earth*, Vol. 89, No. B5, pp. 3193-3200. DOI: 10.1029/ JB089iB05p03193

[31] Escario, V. and Saez, J., 1986. The shear strength of partly saturated soils. *Géotechnique*, Vol. 36, No. 3, pp. 453-456. DOI: 10.1680/geot. 1986.36.3.453

[32] ASTM., 2014. Standard practices for preserving and transporting soil samples. D4220/D4220-M14 (PA USA: American Society for Testing and Materials).

[33] SANS., 2010. Determination of the moisture content by oven-drying. SANS 3001 Part GR20 (Pretoria: SABS standards division).

[34] ASTM., 2004. Standard test methods for particle-size distribution (gradation) of soils using sieve analysis. D6913–04 (PA USA: American Society for Testing and Materials).

[35] ASTM., 2016. Standard test method for particle-size distribution (gradation) of fine-grained soils using the sedimentation (hydrometer) analysis. D7928-16 (PA USA: American Society for Testing and Materials).

[36] ASTM., 2014. Standard test method for the specific gravity of soils. D854-14 (PA USA: American Society for Testing and Materials).

[37] ASTM, 2005. Standard test method for liquid limit, plastic limit, and plasticity index of soils. D4318-05 (PA USA: American Society for Testing and Materials).

[38] BIS, I., 1977. Methods of test for soils: IS 2720-Part 40 Determination of free swell index of soils, pp. 1-5 (New Delhi: Bureau of Indian standards).

[39] Sridharan, A. and Prakash, K., 2000. Classification procedures for expansive soils. *Proceedings of the Institution of Civil Engineers-Geotechnical Engineering*, Vol. 143, No. 4, pp. 235-240

[40] SANS, 2015. Civil engineering test methods, determination of the maximum dry density and optimum moisture content. SANS 3001 Part GR30 (Pretoria: SABS standards division).

[41] Brindley, G.W. and Brown, G., 1984. Crystal structures of clay minerals and their x-ray diffraction identification. *London: Mineralogical Society. 495 p*.

[42] ASTM., 2016. Standard test method for measurement of soil potential (suction) using filter paper. D5298-16 (PA USA: American Society for Testing and Materials).

[43] Van Genuchten, M.T., 1980. A closed-form equation for predicting the hydraulic conductivity of unsaturated soils 1. *Soil science society of America* journal, Vol. 44, No. 5, pp. 892-898.

[44] Kosugi, K.I., 1996. Lognormal distribution model for unsaturated soil hydraulic properties. *Water Resources Research*, Vol. 32, No. 9, pp. 2697-2703.

[45] Fredlund, D.G. and Xing, A., 1994. Equations for the soil-water characteristic curve. *Canadian geotechnical journal*, Vol. 31, No. 4, pp. 521-532. DOI: 10.1139/t94-061

[46] Seki, K., 2007. SWRC fit–a nonlinear fitting program with a water retention curve for soils having unimodal and bimodal pore structure. *Hydrology and Earth System Sciences Discussions*, Vol. 4, No. 1, pp. 407-437. DOI: 10.5194/hessd-4-407-2007

[47] CSIR Transportek., 2002. Protocols for Triaxial Testing: Technical Report TR 2002/21, CSIR, Pretoria, South Africa.

[48] Tarantino, A. and De Col, E., 2008. Compaction behaviour of clay. *Geotechnique,* Vol. 58, No. 3, pp. 199-213.

[49] Naderi, N., Roshani, P., Samani, M.Z. and Tutunchian, M.A., 2012. Application of genetic programming for estimation of soil compaction parameters. In *Applied Mechanics and Materials*, 147: 70-74. DOI: 10.4028/www.scientific.net/AMM.147.70

[50] Đoković, K., Rakić, D. and Ljubojev, M., 2013. Estimation of soil compaction parameters based on the Atterberg limits. *Mining and Metallurgy Engineering Bor*, Vol. 4, pp. 1-16.

[51] Shien, N.G.K., Chew, Y.M., Osman, M.H. and Ghazali, S.K., 2015. Estimating maximum dry density and optimum moisture

content of compacted soils. In *Proceedings of the International Conference on Advances in Civil and Environmental Engineering, Pulau Pinang, Malaysia*.

[52] Fondjo, A.A., Theron, E. and Ray, R.P., 2021. Semi-Empirical model for predicting the swelling stress of compacted, unsaturated expansive soils. *Civil Engineering and Architecture* Vol. 9, No. 1, pp. 225-239. DOI: 10.13189/cea.2021.090119

[53] Fondjo, A.A. and Theron, E. and Ray, R.P., 2021. Estimation of Optimum Moisture Content and Maximum Dry Unit Weight of Fine-Grained Soils using Numerical Methods. *Walailak Journal of Science and Technology,* Vol. 18, No. 16, Article 22792. DOI: 10.48048/wjst.2021.22792

[54] Fondjo, A.A., Theron, E. and Ray, R.P., 2021. Investigation of the influencing soil parameters on the air entry values in soil-water characteristic curve of compacted, heaving soils. *Civil Engineering and Architecture*. Vol. 9, No. 1, pp. 91-114. DOI: 10.13189/cea.2021.090108

[55] Fondjo, A.A. and Theron, E., 2021. Application of mathematical function to estimate the compaction characteristics of unsaturated soils. *Civil Engineering and Architecture*. Vol. 9, No. 1, pp. 255 - 262. DOI: 10.13189/cea.2021.090121

[56] Rao, S.M. and Revanasiddappa, K., 2000. Role of matric suction in collapse of compacted clay soil. *Journal of Geotechnical and Geoenvironmental Engineering*, Vol. 126, No.1, pp. 85-90. DOI: 10.1061/(ASCE)1090-0241(2000)126:1(85)

[57] Fondjo, A.A. and Dzogbewu, T.C., 2019. Assessment of stress raiser factor using finite element solvers. *Universal Journal of Mechanical Engineering*, Vol. 7, No. 6, pp. 367 - 379. DOI: 10.13189/ujme.2019.070608

[58] Fondjo, A.A., Theron, E. and Ray, R.P., 2020. Assessment of various methods to measure the soil suction. *International Journal of Innovative Technology and Exploring Engineering*, Vol. 9, No. 12, pp. 171-184. DOI: 10.35940/ijitee.L7958.1091220

[59] Leong, E.C., Tripathy, S. and Rahardjo, H., 2003. Total suction measurement of unsaturated soils with a device using the chilled-mirror dew-point technique. *Geotechnique*, Vol. 53, No. 2, pp.173-182. DOI: 10.1680/geot.2003.53.2.173

[60] Fredlund, D.G. and Rahardjo, H., 1993. *Soil mechanics for unsaturated soils*. John Wiley & Sons.

[61] Likos, W.J, Wayllace A, Godt, J. and Lu, N., 2010. Modified direct shear apparatus for unsaturated sand at low suction and stress. *Geotechnical Testing Journal*, Vol. 33, No.4, pp.1-13.

[62] Nam, S, Gutierrez, M, Diplas, P. and Petrie, J., 2011. Determination of the shear strength of unsaturated soils using the multistage direct shear test. Eng. Geol. Vol. 122, No. 3-4, pp. 272–280.

[63] Kalaycı, Ş., 2010. *SPSS uygulamalı çok değişkenli istatistik teknikleri.* Translation: SPSS applied multivariate statistical techniques, Vol. 5, pp. 359. Ankara, Turkey: Asil Publication Distribution

[64] Oyediran, I.A. and Durojaiye, H.F., 2011. Variability in the geotechnical properties of some residual clay soils from south western Nigeria. *International Journal of Scientific & Engineering Research*, Vol. 2, No. 9, pp.1-6.

[65] Huzhu, Z., Hanbing, L., Jing, W. and Weizhi, D., 2017. Investigation of the effect of water content and degree of compaction on the shear strength of clay soil material. *Functional materials*. Vol. 24, No.2. DOI: 10.15407/fm24.02.290

[66] Zhao, Y., Duan, X., Han, J., Yang, K. and Xue, Y., 2018. The main influencing factors of soil mechanical characteristics of the gravity erosion environment in the dry-hot valley of Jinsha river. *Open Chemistry*, Vol. 16, No. 1, pp. 796-809.

[67] Wang, G.Y., Huang, Y.G., Li, R.F., Chang, J.M. and Fu, J.L., 2020. Influence of vetiver root on strength of expansive soil-experimental study. *PLoS One*, Vol.15, No. 12.

[68] Mousavi, S.M., Alavi, A.H., Gandomi, A.H. and Mollahasani, A., 2011. Nonlinear genetic-based simulation of soil shear strength parameters. *Journal of earth system science*, Vol. 120, pp.1001-1022.

[69] Akayuli, C., Ofosu, B., Nyako, S.O. and Opuni, K.O., 2013. The influence of observed clay content on shear strength and compressibility of residual sandy soils. *International Journal of Engineering Research and Applications*, Vol. 3, No. 4, pp. 2538-2542.

[70] Ranjan, G. and Rao, A.S.R., 2007. *Basic and applied soil mechanics*. New Age International (P) Ltd., Publishers, New Delhi.

[71] Dafalla, M.A., 2013. Effects of clay and moisture content on direct shear tests for clay-sand mixtures. *Advances in Materials Science and Engineering*. DOI: 10.1155/2013/562726

[72] Ojuri, O.O., 2013. Predictive shear strength models for tropical lateritic soils. Journal *of Engineering*. DOI: 10.1155/2013/595626

[73] Deliktaş, C., 2016. Influence of swell on shear strength of expansive soils. Master Thesis, Graduate School of Natural and Applied Science, Middle East Technical University.

[74] Al-Mhaidib, A.I. and Al-Shamrani, M.A., 2000. Influence of swell on shear strength of expansive soils. Paper presented at the ISRM International Symposium, Melbourne, Australia, November 2000. ISRM-IS-2000-204.

[75] Bláhová, K., Ševelová, L. and Pilařová, P., 2013. Influence of water content on the shear strength parameters of clayey soil in relation to stability analysis of a hillside in Brno region. *Acta Universitatis Agriculturae et Silviculturae Mendelianae Brunensis*, Vol. 61, No. 6, pp.1583-1588.

[76] Tafari, T., Quezon, E.T. and Yasin, M., 2021. Statistical Analysis on Shear Strength Parameter from Index Properties of Fine-grained Soils. *Journal of Engineering Research and Reports*. Vol. 20, No. 4, pp. 15-28.

[77] Durner, W., 1994. Hydraulic conductivity estimation for soils with heterogeneous pore structure. *Water resources research*, Vol. 30, No. 2, pp. 211-223. DOI: 10.1029/93WR02676

[78] Fondjo, A. A., Vuwane, B. and Theron, E., 2023. Improvement of Geotechnical Properties of Heaving Soils Using Alternative Methods: A Review. *Theory and Applications of Engineering Research*, Vol. 1, pp. 127–149. DOI: 10.9734/bpi/taer/v1/8150A

[79] Fondjo, A.A., Theron, E. and Ray, R.P., 2024. Unsaturated shear strength assessment based on soil index properties. *Theory and Applications of Engineering Research Vol. 2*, pp. 67-94. DOI: 10.9734/bpi/taer/v2/8340A

[80] Terzaghi, K. 1936. The shear strength of saturated soils. In *Proceedings. 1st International Conference in Soil Mechanics and Foundation Engineering,* (Vol. 1, pp. 54-56). Cambridge.

[81] Mohr, H. 1914. *Geologie der Wechselbahn (insbesondere des grossen Hartbergtunnels)*. Vienna-Kais. Akad. d. Wissensch.

Appendix 1

Table 1: Sampling location coordinates.

Samples	Global positioning system
BFS	29° 05'30,50''S / 26° 07'46,60''E
WES	27° 57'51,80''S / 26° 45'36,90''E
WIS	28° 30'43,50''S / 27° 00'12,80''E
BES	28° 13'23,40''S / 28° 19'23,00''E

Table 2: Swelling potential classification [39].

FSR	Clay type	Soil expansivity	Dominant clay mineral type
=1	Non-swelling	Negligible	Kaolinite
1.0 –1.5	Mixture of swelling and non-swelling	Low	Mixture of Kaolinitic and Montmorillonitic
1.5 – 2.0	Swelling	Moderate	Montmorillonitic
2.0 – 4.0	Swelling	High	Montmorillonitic
> 4.0	Swelling	Very high	Montmorillonitic

Table 4: Swelling potential test results.

Soil	Swelling potential Classification IS 2720 - 40 (1977) [38]		Swelling potential classification, Sridharan & Prakash (2000) [39]	
	(FSI[1]), %	Soil expansivity	(FSR[2])	Soil expansivity
BFS	64.31	Moderate	1.64	Moderate
WIS	81.37	Moderate	1.73	Moderate
WES	116.60	High	2.20	High
BES	35.81	Moderate	1.17	Low

[1]FSI: free swell index.
[2]FSR: free swell ratio

Table 5: Compaction characteristics.

Soil	OWC (%)	γ_{dmax} (kN/m^3)
BFS	20.10	17.60
WIS	24.00	16.90
WES	26.10	16.30
BES	17.20	19.60

Table 6: X-ray diffraction results.

Soils	Smectite (%)	Silica (%)	Group of feldspar minerals		Illite (%)	Calcite (%)
			K-feldspar (%)	Plagioclase (%)		
BFS	56.83	12.47	23.51	3.29	1.89	2.01
WIS	58.22	25.08	10.42	2.45	2.02	trace
WES	67.05	19.98	10.66	2.31	trace	trace
BES	31.67	31.39	21.22	8.15	3.36	4.21

Appendix 2

Table 7: Suction test results.

Soils	Soil water content (%)	Dry unit weight, (kN/m^3)	Total suction (kPa)	Matric suction (kPa)	Osmotic suction (kPa)	Air entry value (kPa)
BFS	12.06	15.60	5883.92	4741.62	1142.3	
	14.02	16.21	4064.22	3327.18	737.04	10
	17.03	17.01	1923.09	1388.22	534.87	
	20.07	17.58	1036.11	671.89	364.22	
	24.8	17.20	340.034	200	140.034	
WIS	14.98	15.60	7439.15	5984.56	1454.59	
	17.50	16.05	5410.66	4332.678	1077.982	14.82
	21	16.58	3580.89	2748.30	832.59	
	24.03	16.85	1699.05	1199.35	499.70	
	28.06	16.70	816.77	450.227	366.543	
WES	15.93	14.94	9926.183	7693.666	2232.517	
	19.25	15.48	6922.321	5227.777	1694.544	16.13
	23.37	16.09	4011.482	2986.456	1025.026	
	26.14	16.29	2475.62	1778.651	696.969	
	29.10	15.85	1397.745	890.47	507.275	
BES	9.18	16.35	4163.35	3312.26	851.09	
	12.42	18.01	2510.04	1982.31	527.73	6.00
	14.54	18.95	830.926	538.11	292.816	
	17.23	19.60	323.818	225.609	98.209	
	20.30	19.10	109.66	79.70	29.96	

Table 8: Unsaturated shear strength parameters.

Soil	Water content (%)	c' (kPa)	tan (ϕ') (Degree)	(σ_n-u_a) (kPa)	τ_s (kPa)	(u_a-u_w) (kPa)	tan (ϕ^b) Degree	τ_u (kPa)	τ_u/τ_s
BFS	12.06	75.05	52.09	605.5	853	4741.62	6.77	1414.44	1.66
	14.02	72.05	48.55	547.78	692	3327.18	6.77	1086.56	1.57
	17.03	67.11	44.65	485.53	547	1388.22	6.77	711.25	1.30
	20.07	58.10	39.66	406.30	395	671.89	6.77	474.56	1.20
	24.80	51.54	32.71	333.87	266	200	6.77	289.67	1.09
WIS	14.98	69.42	50.75	537.59	727	5984.56	5.02	1253.44	1.72
	17.50	63.89	47.18	492.32	595	4332.68	5.02	976.02	1.64
	21	57.95	42.75	423.28	449	2748.30	5.02	690.80	1.54
	24.03	55.60	37.21	365.56	333	1199.35	5.02	438.60	1.32
	28.06	49.30	32.51	282.94	230	450.23	5.02	269.20	1.17
WES	15.93	62.39	42.07	452.71	471	7693.67	2.67	830.31	1.76
	19.25	57.32	37.95	413.10	379	5227.78	2.67	623.62	1.65
	23.37	50.11	34.31	328.78	274	2986.46	2.67	413.94	1.51
	26.14	48.85	28.8	284.07	205	1778.65	2.67	288.08	1.41
	29.1	45.31	24.92	234.84	154	890.47	2.67	196.01	1.27
BES	9.18	78.34	53.21	645.11	941	3312.26	10	1512.02	1.61
	12.42	69.05	50.08	554.57	732	1982.31	10	1073.58	1.47
	14.54	64.56	46.03	503.07	586	538.11	10	678.82	1.16
	17.23	61.09	42.42	431.77	456	225.61	10	494.52	1.08
	20.3	54.93	33.05	350.85	283	79.70	10	296.95	1.05

Appendix 3

Table 9: Degrees of correlation between dependent variables (Kalayci, 2010) [63].

Coefficient of correlation (R^2)	Degrees of correlation
0.00 – 0.25	Very weak correlation
0.26 – 0.49	Weak correlation
0.50 – 0.69	Moderate correlation
0.70 – 0.89	Strong correlation
0.90 –1.00	Very strong correlation

Table 10: ϕ‘ relationship with soil properties’ equations.

Correlation equations	R^2	Equation number
$\phi' = 3739.6e^{-1.753Gs\ (\%)}$	0.72	11
$\phi' = 82.81e^{-0.04W\ (\%)}$	0.71	12
$\phi' = 68.87e^{-0.012LL\ (\%)}$	0.68	13
$\phi' = 51.04e^{-0.011PI\ (\%)}$	0.64	14
$\phi' = 73.63e^{-0.012Fine\text{-}grained\ (\%)}$	0.72	15
$\phi' = 52.34e^{-0.014Clay\ (\%)}$	0.74	16
$\phi' = 5.059e^{0.108gd\ (kN/m3)}$	0.62	17
$\phi' = 57.16e^{-0.932Void\ ratio}$	0.69	18
$\phi' = 63.49e^{-0.368FSR}$	0.74	19
$\phi' = 46.72e^{-0.004FSI\ (\%)}$	0.70	20
$\phi' = 56.134e^{-0.01Smectite\ (\%)}$	0.61	21
$\phi' = 26.81e^{0.0574\ Plagioclase\ (\%)}$	0.53	22

Table 11: ϕ^b relationship with soil properties’ equations.

Correlation equations	R^2	Equation number
$\phi^b = 106.51e^{-0.05Fine\ content\ (\%)}$	0.92	23
$\phi^b = 27.04e^{-0.054Clay\ (\%)}$	0.92	24
$\phi^b = 84.48e^{-0.048LL\ (\%)}$	0.93	25
$\phi^b = 25.95e^{-0.046PI\ (\%)}$	0.92	26
$\phi^b = 5.E+08e^{-6.883Gs}$	0.88	27
$\phi^b = 0.0022e^{0.438gd\ (kNm3)}$	0.81	28
$\phi^b = 166.47e^{-0.161W\ (\%)}$	0.88	29
$\phi^b = 20.29e^{-0.119AEV\ (kPa)}$	0.92	30
$\phi^b = 18\ e^{-0.018FSI\ (\%)}$	0.93	31
$\phi^b = 37.03e^{-0.038Smectite\ (\%)}$	0.79	32
$\phi^b = 1.884e^{0.229Plagiocalse\ (\%)}$	0.67	33
$\phi^b = 1.167e^{0.0833K\text{-}feldspar\ (\%)}$	0.66	34

Appendix 4

Table 12: c' relationship with soil properties' equations.

Correlation equations	R^2	Equation number
$c' = 98.71e^{-0.03W\ (\%)}$	0.73	35
$c' = 1887e^{-1.341Gs}$	0.71	36
$c' = 86.53e^{-0.009LL\ (\%)}$	0.61	37
$c' = 69.26e^{-0.008PI\ (\%)}$	0.56	38
$c' = 91.84e^{-0.009Fine\ content\ (\%)}$	0.68	39
$c' = 71.59e^{-0.01Clay\ (\%)}$	0.71	40
$c' = 75.759e^{-0.629Void\ ratio}$	0.63	41
$c' = 13.201e^{0.0776gd\ (kN/m3)}$	0.54	42
$c' = 73.71e^{-0.007Smectite\ (\%)}$	0.52	43
$c' = 65.22e^{-0.003FSI\ (\%)}$	0.62	44
$c' = 39.19e^{0.0162K\text{-}feldspar\ (\%)}$	0.53	45
$c' = 43.63e^{0.0407Plagioclase\ (\%)}$	0.50	46

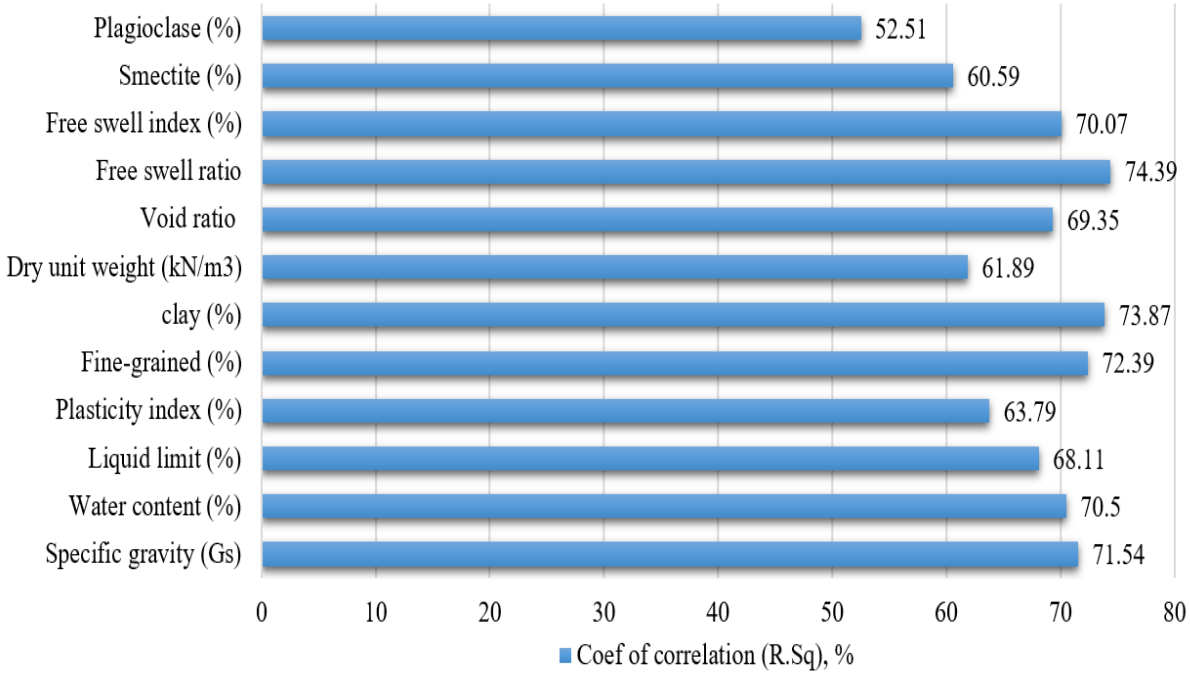

Figure 37 Correlation diagram of ϕ' and the soil properties.

Appendix 5

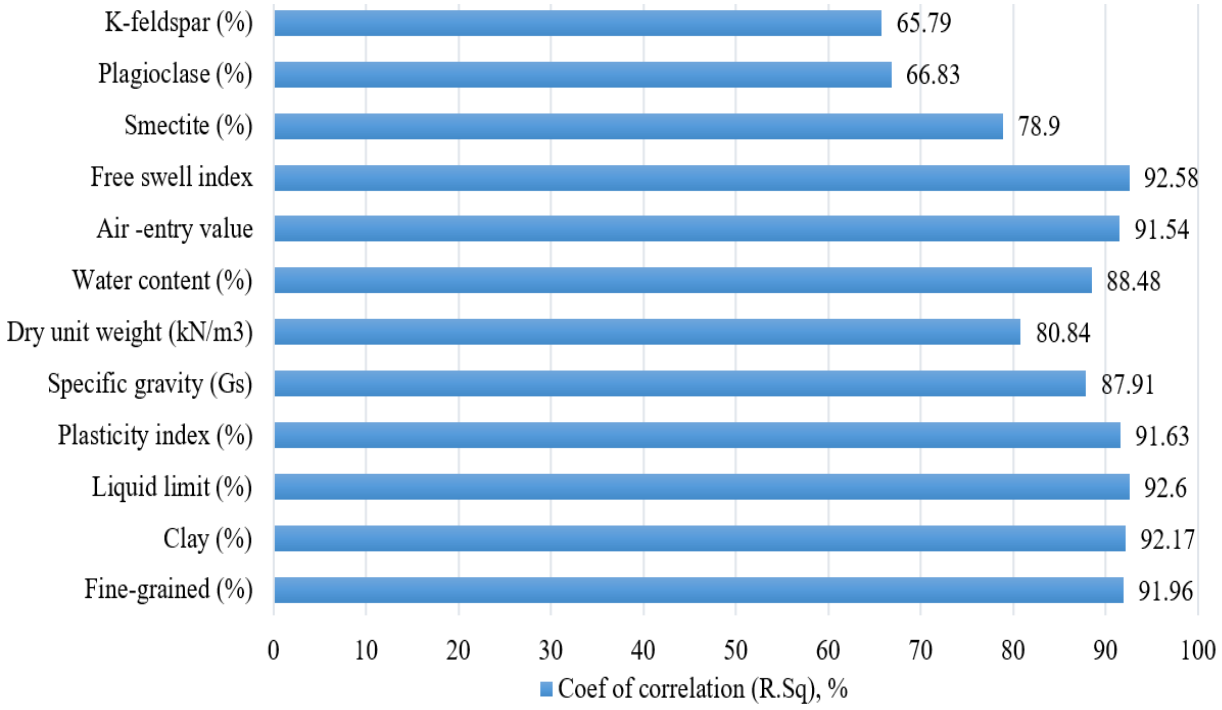

Figure 38: Correlation diagram of ϕ^b and the soil properties.

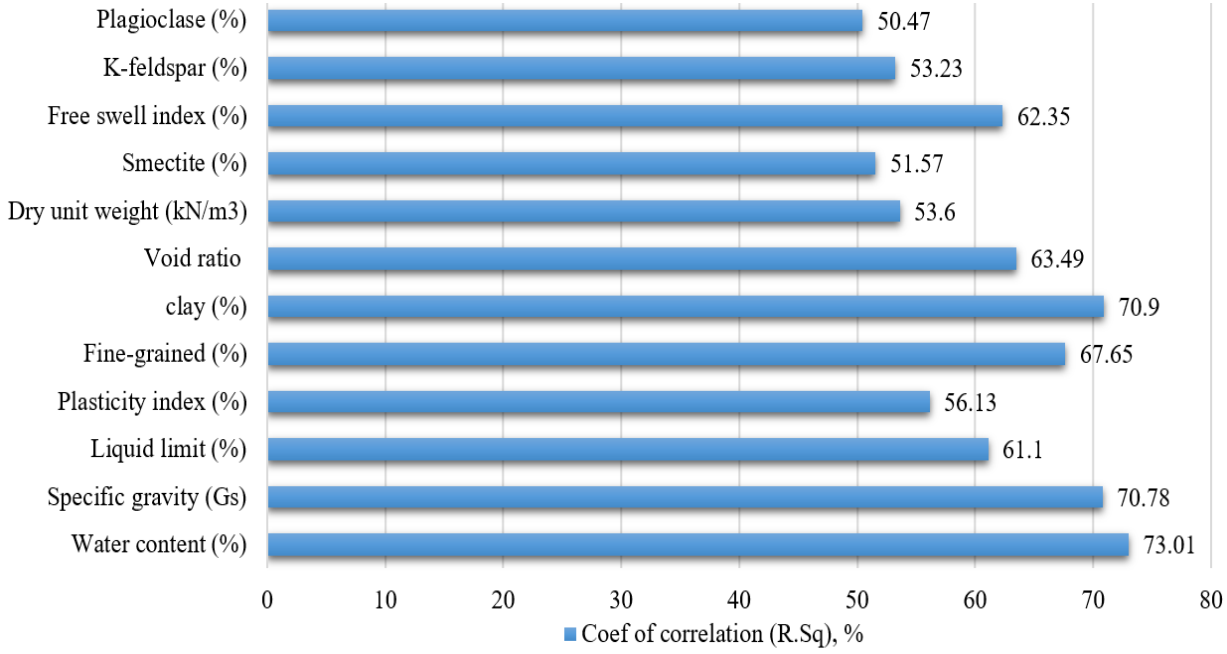

Figure 39: Correlation diagram of c‘ and the soil properties.

Appendix 6

Table 13: Shear strength equations of saturated and unsaturated soils.

Authors	Equation	Number
Terzaghi [80]	$\tau_s = c' + (\sigma_n - u_w)\tan(\phi')$	1
Fredlund and Rahardjo [60]	$\tau_u = c' + (\sigma_n - u_a)\tan(\phi') + (u_a - u_w)\tan(\phi_b)$	2
Vanapalli *et al.* [27]	$\tau_u = c' + (\sigma_n - u_a)\tan(\phi') + \left(\frac{\theta - \theta_r}{\theta_s - \theta_r}\right)(u_a - u_w)\tan(\phi')$	3
Khalili and Khabbaz [25]	$\tau_u = c' + (\sigma_n - u_a)\tan(\phi') + (\chi)(u_a - u_w)\tan(\phi')$ $\chi = \left[\frac{(u_a - u_w)}{AEV}\right]^{-0.55}$	4
Vanapalli and Fredlund [18]	$\tau_u = c' + (\sigma_n - u_a)\tan(\phi') + \chi(u_a - u_w)\tan(\phi')$ $\chi = (S_r)^k$ $k = 0.98 + 0.0874\,(PI) - 0.001\,(PI)^2$	5
Tekinsoy *et al.* [28]	$\tau_u = c' + (\sigma_n - u_a)\tan(\phi') + \tan(\phi')\,(AEV + Pat)\ln\left[\frac{(u_a - u_w) + P_{at}}{P_{at}}\right]$	6
Garven and Vanapalli [19]	$\tau_u = c' + (\sigma_n - u_a)\tan(\phi') + \theta^k (u_a - u_w)\tan(\phi')$ $k = 0.00161\,PI^2 + 0.0975\,PI + 1$	7
Guan *et al.* [29]	$\tau_u = c' + (\sigma_n - u_a)\tan(\phi') + (u_a - u_w)\tan(\phi^b)$ where $\phi^s = \phi^b$ if $(u_a - u_w) < AEV$ $\tau_u = c' + [(\sigma_n - u_a) + AEV]\tan(\phi') + [(u_a - u_w) - AEV]\, b\theta^k \tan(\phi')$ if $(u_a - u_w) \geq AEV$ $k = [\log(u_a - u_w) - \log(AEV)]^y$ For drying: $y_d = 0.502\ln(PI + 2.7) - 0.387$ $b_d = -0.254\{\ln[n_d\,(PI + 4.4)] - 0.387\}^2 + 2.114\,\{\ln[n_d\,(PI + 4.4)]\} - 3.522$ For wetting: $y_w = 3.55\,y_d - 3.00$ $b_w = 0.542\,b_d\,(n_d/n_w) + 0.389$	8

Appendix 7

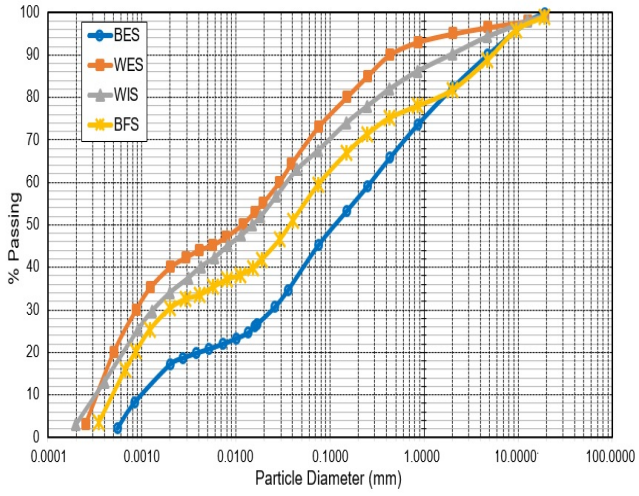

Figure 25: Grain size distribution curves of four soil samples

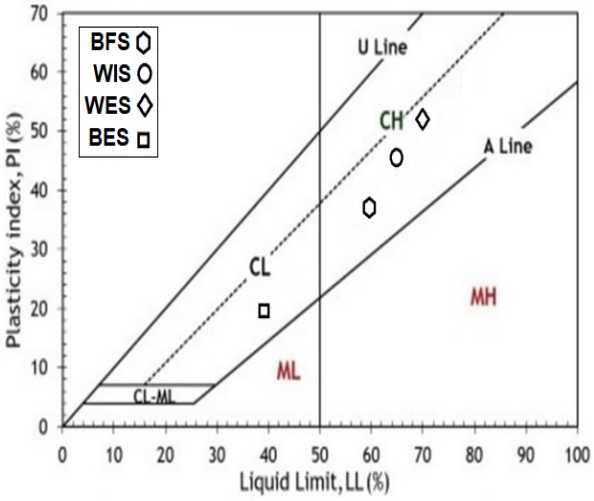

Figure 26: Plasticity chart of four soil samples

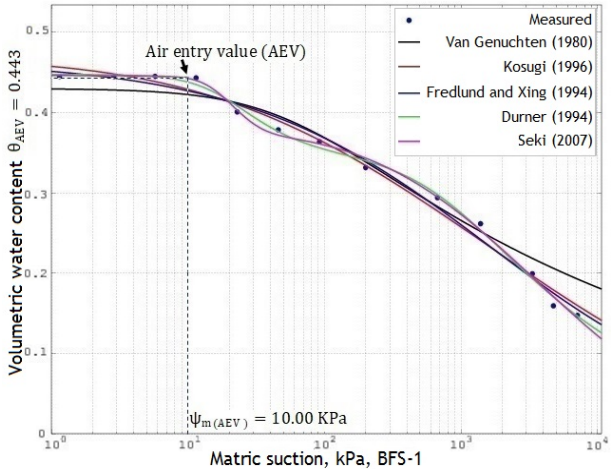

Figure 27: Soil–water characteristic curve for BFS as compacted

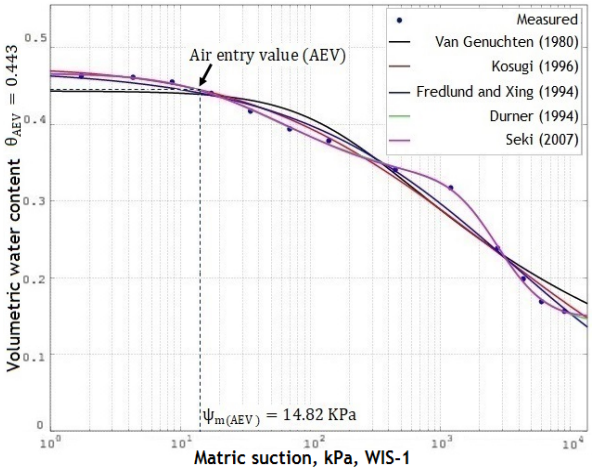

Figure 28: Soil–water characteristic curve for WIS as compacted

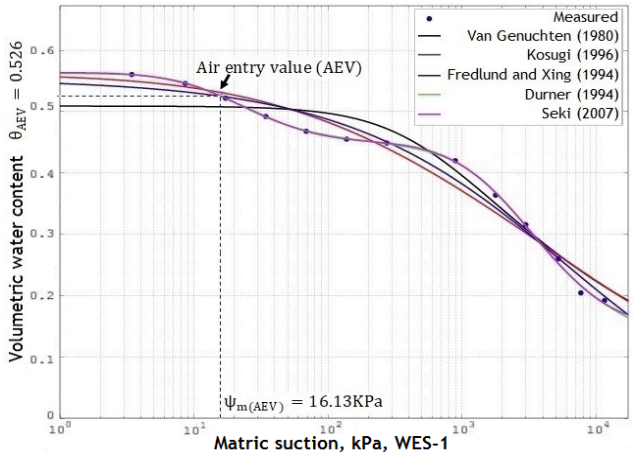

Figure 29: Soil–water characteristic curve for WES as compacted

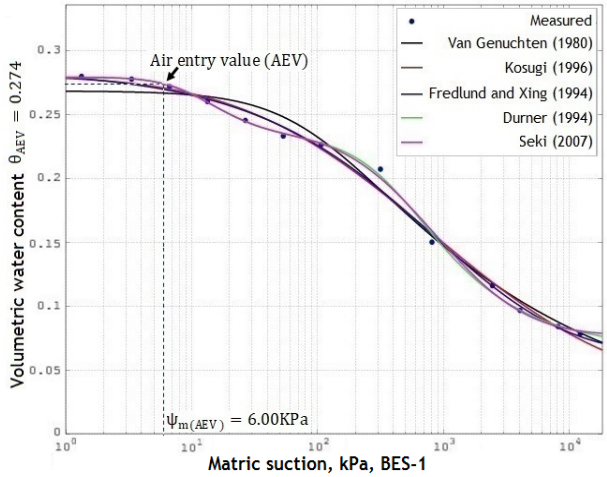

Figure 30: Soil–water characteristic curve for BES as compacted

Appendix 8

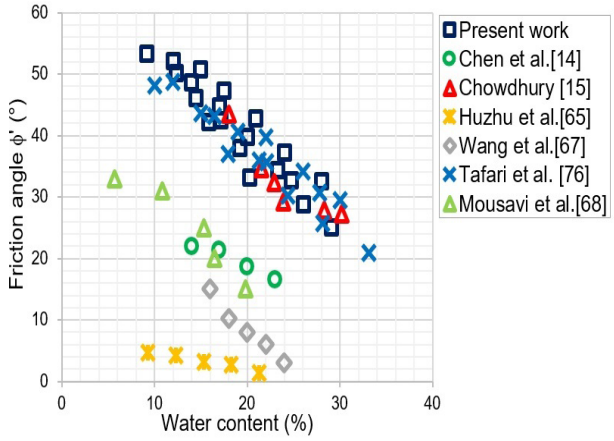

Figure 31: Graph of correlations between friction angle (ϕ‘) and water content.

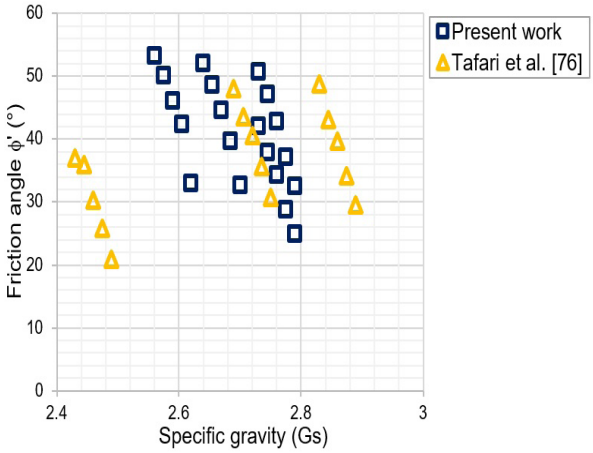

Figure 32: Graph of relationships between friction angle (ϕ‘) and specific gravity (Gs).

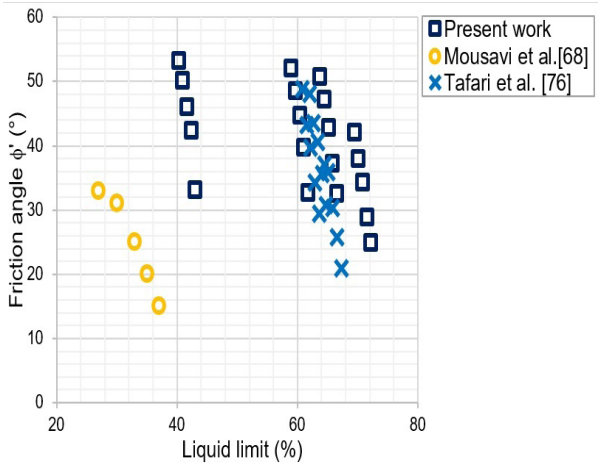

Figure 33: Graph of correlations between friction angle (ϕ‘) and liquid limit (LL).

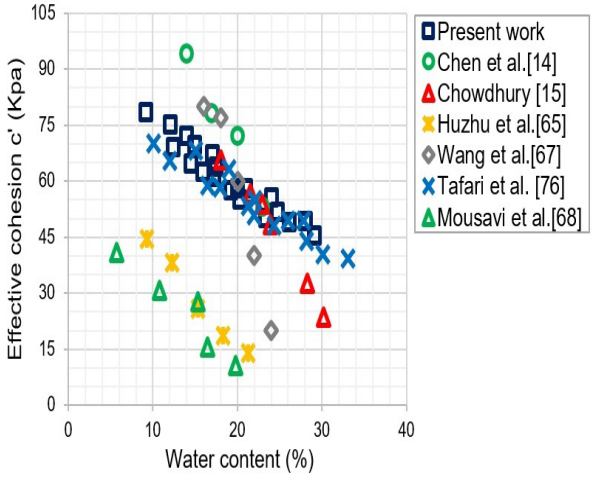

Figure 34: Graph of relationships between effective cohesion (c‘) and water content.

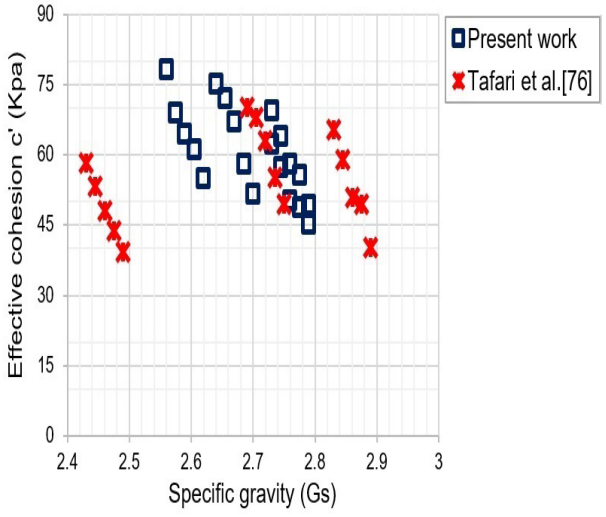

Figure 35: Graph of correlations between effective cohesion (c‘) and specific gravity (Gs).

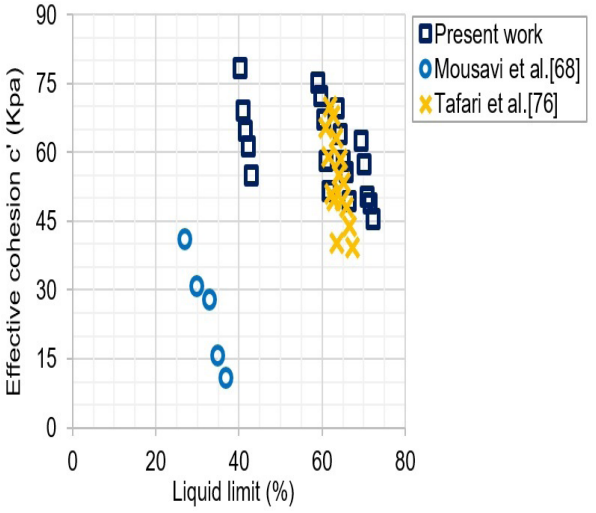

Figure 36: Graph of relationships between effective cohesion (ϕ') and liquid limit (LL).